A Novel IPT Converter With Current-Controlled Semi-Active Rectifier for Efficiency Enhancement Throughout Supercapacitor Charging Process

Zhicong Huang, *Member, IEEE*, Dule Wang, and Xiaohui Qu, *Senior Member, IEEE*

***Abstract*— During the typical constant current (CC) charging process, the supercapacitor has a pretty wide-range load variation. However, an inductive power transfer (IPT) converter can maintain high efficiency only within a certain load range around its optimum load point. Once the supercapacitor load resistance is far away from the optimum point, which usually happens in low charging power levels, i.e., the smaller load resistances, the IPT converter will suffer from the dramatic efficiency degradation and thus a step-up load transformation is required throughout the whole charging process. In this article, a novel current-controlled semi-active rectifier (CCSAR)-based IPT converter is proposed to fulfill this requirement. The characteristic of step-up load transformation is first identified and implemented by controlling the conduction angle of the CCSAR to enhance the efficiency in the charging process. The desired charging CC is then regulated by tuning the operating frequency of the IPT inverter. To coordinate these two objectives, a bivariate control is adopted here to achieve fast, direct, and precise current output with enhanced efficiency performance over the whole load range during the CC charging process. Finally, experiment results validate the theoretical analysis well.**

***Index Terms*— Bivariate control, constant current (CC) charging, efficiency enhancement, inductive power transfer (IPT), supercapacitor.**

I. Introduction

DEVELOPMENT in modern power electronics has enabled inductive power transfer (IPT) technologies well, which can transfer power wirelessly over a short-range air gap without physical contact [1]. Compared with conventional conductive power transfer using plugs and cables, IPT has shown significant advantages in providing user-friendly and maintenance-free operations to recharge consumer electronics, biomedical implants, and electric vehicles [2]–[7]. In these applications, emerging supercapacitors are being more and more attractive because they have longer life duration and faster charging speed without degrading their expected lifetime [8], [9].

Typically, constant current (CC) charging plays a dominant stage in the charging profile of supercapacitor [10], [11], and the supercapacitor can be almost fully charged with a single CC charging stage [12]–[14]. During the CC charging to a depleted supercapacitor, the supercapacitor voltage linearly increases from a near-zero value to a voltage limit. Therefore, the supercapacitor can be considered as an equivalent resistance with a wide range variation, i.e., as wide as 0%–100% of voltage limit over charge current. It has been studied that, the maximum efficiency of an IPT converter occurs only at a specified load, thus named as optimum load [15]–[18]. Therefore, efficiency optimization is challenging during the whole charging process of the supercapacitor. An appropriate IPT converter as well as its control method is needed for load matching in the achievement of CC output.

It is an intuitive idea to design a single-stage IPT converter with its inherent CC output characteristic (also called load-independent current output characteristic) for the CC charging [19]–[23]. The single-stage IPT converter can operate at a fixed frequency to provide a substantial CC output, and thus the control effort can be minimized. Design methodologies of different compensation topologies for the IPT converter have been widely studied to customize the CC output [22], [23]. However, such a simple single-stage design cannot achieve high efficiency over the wide load range during the CC charging process, due to the absence of load matching. When the load deviates a lot from the optimum point, usually in the light load conditions, the efficiency of the IPT converter will degrade dramatically.

To achieve the load matching function, multistage IPT systems have been widely studied by using extra dc/dc converters cascaded in the front-end and/or the load-side of the IPT converter [24]–[26]. Then these multistage designs can have more degrees of control freedom for efficiency optimization and power regulation under the supercapacitor charging profile. But there exist some obvious drawbacks, which include more losses, costs, and complicated controllers due to the extra converter stages. To save the converter stage, the modulation given by the extra dc/dc converters can be replaced by the inverter circuit and an active rectifier both with pulsewidth modulation (PWM) in a single-stage IPT converter [14], [27],

Manuscript received April 13, 2021; revised July 17, 2021; accepted August 19, 2021. Date of publication August 24, 2021; date of current version April 4, 2022. This work was supported in part by the National Natural Science Foundation of China under Grant 52007067 and Grant 52077038, in part by Guangzhou Municipal Science and Technology Bureau under Grant 202102020381, in part by the Natural Science Foundation of Jiangsu Province under Grant BK20181280, and in part by the Fundamental Research Funds for Central Universities of China. Recommended for publication by Associate Editor Chi Kwan Lee. *(Corresponding author: Xiaohui Qu.)*

Zhicong Huang is with Shien-Ming Wu School of Intelligent Engineering, South China University of Technology, Guangzhou 510006, China (e-mail: zhiconghuang@scut.edu.cn).

Dule Wang and Xiaohui Qu are with the School of Electrical Engineering, Southeast University, Nanjing 210096, China (e-mail: xhqu@seu.edu.cn).

Color versions of one or more figures in this article are available at https://doi.org/10.1109/JESTPE.2021.3107141.

Digital Object Identifier 10.1109/JESTPE.2021.3107141

[28]. It is known that PWM control will readily lose the soft-switching conditions in a wide load variation for both inverter and active rectifier, thus resulting in heavy losses of hard switching. Chen *et al.* [29], Colak *et al.* [30], and Mishima and Morita [31] give a voltage-controlled semi-active rectifier (VCSAR) in the IPT converters modulated in a soft-switching way, and meanwhile the conduction angle of the VCSAR is controlled to realize the output regulation. To further match the load for efficiency enhancement, Huang *et al.* [32] proposes an improved coordinated control scheme for the IPT converter with VCSAR to maintain a constant voltage (CV) output as well as high efficiency throughout a wide load range. Nevertheless, it should be noted that the load transformation trend of VCSAR is step-down, which is only suitable for efficiency optimization in the achievement of CV like battery charging applications. In the supercapacitor CC charging, the required step-up load transformation cannot be fulfilled by the VCSAR.

To fill the gap, this article proposes a novel IPT converter with a current-controlled semi-active rectifier (CCSAR). The characteristic of step-up load transformation is first identified to enhance the efficiency in the whole charging process. The control method of conduction angle of the CCSAR for both load matching and soft switching is also elaborated in Section II. To comply with the current-source rectifier, the IPT converter must have a secondary capacitor in parallel with the CCSAR, and a simple series-parallel (SP) compensation is used in Section III. To compensate the capacitive reactance generated in the load step-up transformation, the desired charging CC is then regulated by tuning the operating frequency of the IPT inverter as well as keeping the inductive input impedance to guarantee the zero-voltage switching (ZVS) of inverter MOSFETs. In this way, the objectives of efficiency enhancement and output regulation can be fulfilled in a single-stage IPT converter, and the inverter and rectifier are both switched in the soft-switching manner. To coordinate these two control variables of conduction angle of CCSAR and switching frequency of inverter, a bivariate control is adopted to achieve fast, direct, and precise current output with enhanced efficiency performance. Finally, a 100-V/2-A IPT charger prototype is built to verify the theoretical analysis in Section IV. Section V concludes this article.

The major contributions of this article are summarized as follows.

1) The CCSAR is first studied and used in an IPT system, to the best of our knowledge.
2) The difference between the VCSAR and the CCSAR is comprehensively distinguished in terms of their load transformation ability and their applicable scenarios are identified as well.
3) A specified IPT system (SP compensation with CCSAR) is proposed with a bivariate coordinated control scheme. The proposed system features: 1) CC charging; 2) efficiency optimization throughout the whole CC charging process; 3) soft switching; and 4) single-stage design, which have not yet been studied simultaneously.

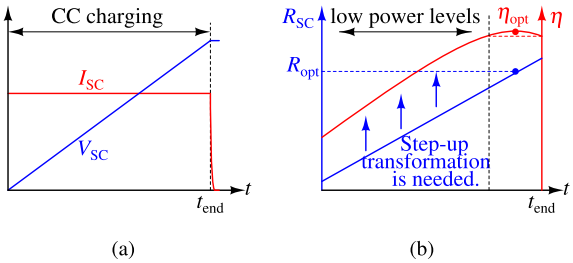

Fig. 1. (a) Typical charging profile of supercapacitor. (b) Diagram of efficiency curve of IPT converter without load matching.

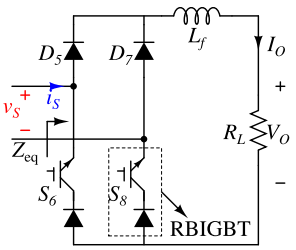

Fig. 2. Schematic of CCSAR.

II. CCSARs and Its Step-Up Load Transformation

In the typical CC charging profile shown in Fig. 1(a), the equivalent load resistance of the supercapacitor donated by $R_{SC} = (V_{SC}/I_{SC})$ increases with time, as shown by the blue solid curve in Fig. 1(b). During the whole charging process, R_{SC} ranges from a near-zero value at the beginning to the maximum at the charging completion t_{end}. It has been studied that the IPT converter only has maximum efficiency η_{opt} at its optimum load resistance, donated by R_{opt}, and it can only maintain relatively high efficiency within a certain range around R_{opt} [20]–[22]. As illustrated by Fig. 1(b), although the IPT can achieve high efficiency at high charging power levels with large R_{SC} close to R_{opt}, it still suffers from significant efficiency degradation when R_{SC} deviates from R_{opt}, especially at light charging power levels. To address this issue, the IPT converter should have the ability to transform R_{SC} in a step-up direction for efficiency enhancement, as indicated by the blue arrows shown in Fig. 1(b).

Semi-active rectifier (SAR) is a full-wave half-controlled bridge converter that includes two active switches and two diodes in the form of a full bridge configuration. It can be classified as VCSAR and CCSAR, depending on controlling the conduction angle of the input voltage or the input current fed to the rectifier. Based on the aforementioned studies [28]–[32], VCSAR modulates the phase angle of input voltage, resulting in the load resistance in a step-down direction, which disobeys the required load transformation indicated in Fig. 1(b). Therefore, as a duality of VCSAR, CCSAR should modulate the conduction angle of input current, so that a step-up load transformation is expected as well as its utilization in the IPT converter for efficiency enhancement.

Fig. 2 gives a typical schematic of CCSAR, where v_S and i_S represent the ac inputs fed to the CCSAR. With the current source characteristic, a series inductor filter L_f is used in the CCSAR. The full bridge configuration of the CCSAR

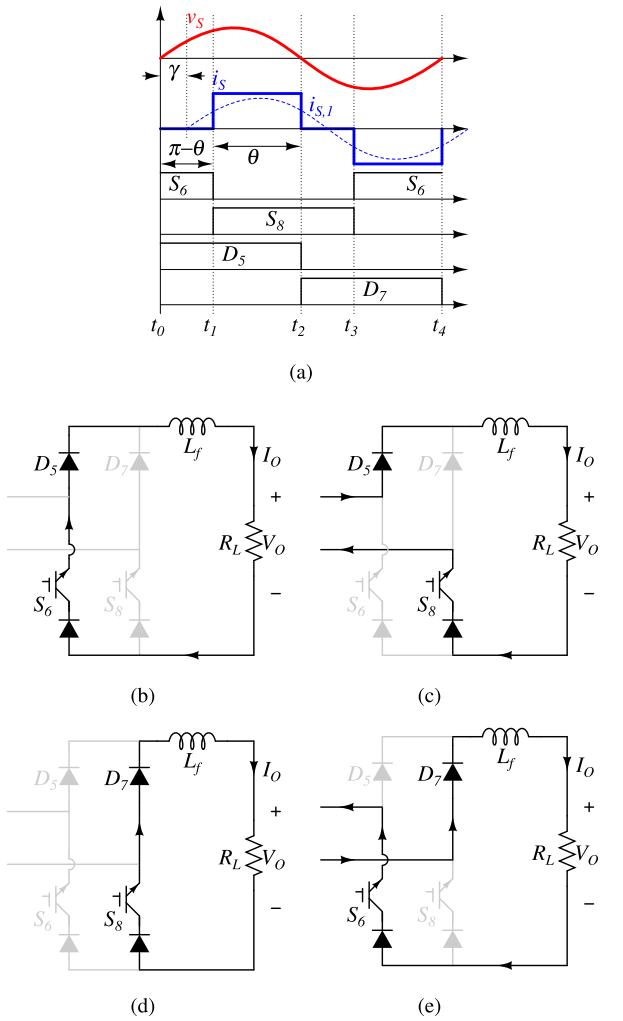

Fig. 3. (a) Switching sequence and operating waveforms. (b)–(e) Key states.

consists of two diodes D_5 and D_7 in the upper legs, and two active switches S_6 and S_8 in the lower legs. S_6 and S_8 should perform the open-circuit of the CCSAR input terminal and then cut off the power flow to the load. Both MOSFET and IGBT have no capability of reverse current blocking due to the existence of body diode or paralleled diode, and therefore the emitter of IGBT or the source of MOSFET should connect cathodes of D_5 and D_7. To avoid the current circulating between S_6 and S_8 under the ON-state of one switch, the anti-series diode is needed in Fig. 2. Zero current switching (ZCS) is particularly effective in reducing switching loss for IGBT switches with a large tail current in the turn-off process [33]. Also, if S_6 and S_8 adopt IGBT, IGBT with the anti-series diode actually performs a reverse blocking IGBT (RBIGBT), which is being commercially available and can eliminate the need for extra anti series diodes [34], [35].

The switching sequence in the CCSAR is shown in Fig. 3(a). Both S_6 and S_8 are ON for half a cycle and they are the complement of each other. S_6 and S_8 are turned off with a time delay of $\pi - \theta \in [0, \pi]$ to the zero cross points of v_S. From Fig. 3(b)–(e), key circuit states are given here to demonstrate ZCS realization. At the end of $[t_0, t_1]$, a slightly earlier turn-on of S_8 before the turn-off of S_6 permits the zero-current

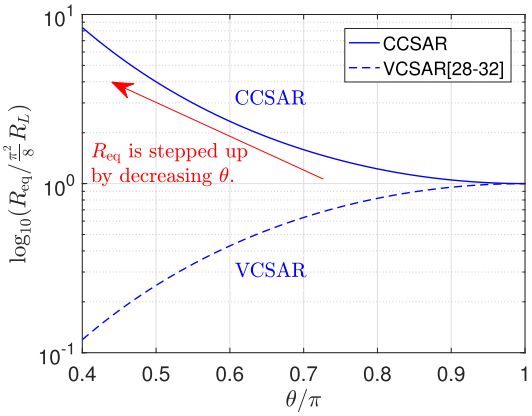

Fig. 4. Inverse trends of load resistance transformation provided by VCSAR [28]–[32] and CCSAR.

switching-off of S_6. Similarly, at the end of $[t_2, t_3]$, a slightly earlier turn-on of S_6 before the turn-off of S_8 guarantees the zero-current switching-off of S_8. As indicated by Fig. 3(a), the conduction angle of i_S is θ, which can be controlled from π to 0. As given in Fig. 3(a), $i_{S,1}$ in the dotted blue line is the fundamental component of i_S that it lags v_S with a phase angle given by $\gamma = (\pi - \theta/2)$. So the change of θ will affect the phase angle between v_S and i_S. Using fundamental approximation [29]–[32], the CCSAR as well as the load can be modeled as an equivalent impedance Z_{eq} that includes a reactive component X_{eq} and a resistive component R_{eq} in parallel connection, given by

$$Z_{eq} = R_{eq} \parallel jX_{eq} \tag{1}$$

where

$$R_{eq} = \frac{\pi^2}{8} R_L \frac{1}{\sin^4\left(\frac{\theta}{2}\right)} \tag{2}$$

$$X_{eq} = \frac{\pi^2}{8} R_L \frac{1}{\sin^3\left(\frac{\theta}{2}\right)\cos\left(\frac{\theta}{2}\right)}. \tag{3}$$

Specially, if $\theta = \pi$ as a diode rectifier, $R_{eq} = (\pi^2/8)R_L$ and $X_{eq} = \infty$. From (2), the load resistance R_{eq} can be modulated in step-up direction by reducing the conduction angle θ. Inverse trends of load resistance transformation provided by the VCSAR and the CCSAR are plotted in Fig. 4. It is clear that the CCSAR is suitable to enhance the efficiency during CC charging for the supercapacitor complying with the requirements of load resistance transformation shown in Fig. 1(b).

However, as indicated in (3), an unexpected load reactance is also generated in the proposed soft-switching modulation, and it is worth further investigating its influence to the output current. Then the corresponding modulation and control for both efficiency enhancement and desired CC output will be discussed in Section III.

III. Proposed IPT System and Bivariate Control for Both Output Regulation and Efficiency Enhancement

A. Characteristic Analysis

Since CCSAR has a sufficiently large inductor filter L_f for maintaining a current source output, the IPT converter

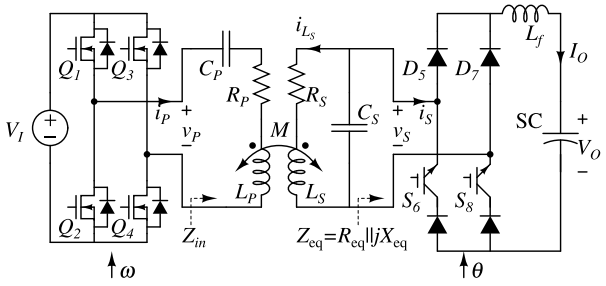

Fig. 5. Proposed CC charging system for supercapacitor based on SP IPT converter with CCSAR.

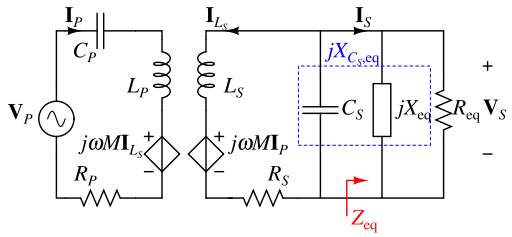

Fig. 6. Equivalent circuit model of the SP IPT converter with CCSAR.

with secondary parallel compensation is suitable to connect such CCSAR. Fig. 5 demonstrates a simplest SP compensation with CCSAR for the supercapacitor charging. C_P and C_S are the primary and secondary compensation capacitors, respectively. The magnetic coupler has self-inductances L_P and L_S with coil parasitic resistances R_P and R_S. The mutual inductance is M and the coupling coefficient is given by $k = (M/(L_P L_S)^{1/2})$. DC voltage V_O and current I_O are the terminal voltage and charging current of the supercapacitor. Since the charging process is slow compared with the resonant period, the supercapacitor can be modeled as a resistor $R_L = (V_O/I_O)$ [32].

With the modeling of the CCSAR in (1), Fig. 6 shows the equivalent model of the proposed SP IPT converter using the fundamental approximation. $\mathbf{V}_P$, $\mathbf{I}_P$, $\mathbf{V}_S$, $\mathbf{I}_{L_S}$, and $\mathbf{I}_S$ are phasors of the fundamental components of v_P, i_P, v_S, i_{L_S}, and i_S, respectively. I_O should be the magnitude of square-wave i_S, which cannot be noted in Fig. 6 with the equivalent model of Z_{eq}. The basic equations are thus given as

$$(jX_P + R_P)\mathbf{I_P} + jX_M\mathbf{I}_{L_S} = \mathbf{V}_P \tag{4}$$

$$-(jX_{L_S} + R_S + jX_{C_{S,eq}} \parallel R_{eq})\mathbf{I}_{L_S} = jX_M\mathbf{I}_P \tag{5}$$

$$-\frac{jX_{C_S}}{jX_{C_S} + jX_{eq} \parallel R_{eq}}\mathbf{I}_{L_S} = \mathbf{I}_S \tag{6}$$

where $X_M = \omega M$, $X_P = \omega L_P - (1/\omega C_P)$, $X_{L_S} = \omega L_S$, $X_{C_S} = -(1/\omega C_S)$, and $X_{C_S,eq} = -(1/\omega C_S) \parallel X_{eq}$.

Without considering the converter losses, the efficiency can be calculated as

$$\eta = \frac{|\mathbf{I}|_S^2 \frac{R_{eq}X_{eq}^2}{R_{eq}^2+X_{eq}^2}}{|\mathbf{I}|_S^2 \frac{R_{eq}X_{eq}^2}{R_{eq}^2+X_{eq}^2} + |\mathbf{I}|_{L_S}^2 R_S + |\mathbf{I}|_P^2 R_P}. \tag{7}$$

Based on the analysis in [24], the optimal efficiency can be achieved when the SP IPT converter is loaded at a purely resistive load given by

$$R_{opt} = \frac{\omega_S L_S^2}{M}\sqrt{\frac{R_P}{R_S}}. \tag{8}$$

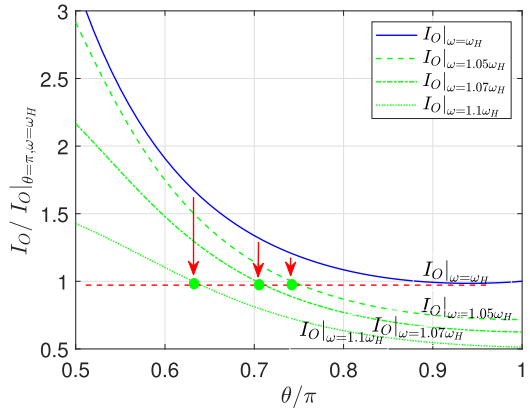

Fig. 7. Normalized I_O versus θ under different operating frequencies.

Using Fourier analysis, the peak magnitudes of $|\mathbf{V}_P|$ and $|\mathbf{I}_S|$ follow that:

$$|\mathbf{V}_P| = \frac{4}{\pi}V_I, \text{ and } |\mathbf{I}_S| = \frac{4}{\pi}\sin\frac{\theta}{2}I_O. \tag{9}$$

Then the dc output current I_O can be calculated as

$$I_O \approx \left|\frac{\frac{jX_{C_{S,eq}}}{jX_{C_{S,eq}}+R_{eq}} \cdot \frac{jX_M}{\sin(\frac{\theta}{2})}}{jX_P(jX_{L_S} + jX_{C_{S,eq}} \parallel R_{eq}) + X_M^2}\right| V_I \tag{10}$$

with R_P and R_S ignored.

In particular, if the CCSAR operates as a passive rectifier, i.e., $\theta = \pi$, with the component losses neglected, two operating frequencies $\omega_{L,H}$ for IPT converter achieving load-independent constant output current can be found from (10), given by

$$\omega_{L,H} = \sqrt{\frac{\omega_P^2 + \omega_S^2 \mp \Delta}{2(1-k^2)}} \tag{11}$$

where $\omega_P = (1/(L_P C_P)^{1/2})$, $\omega_S = (1/(L_S C_S)^{1/2})$, and $\Delta = ((\omega_P^2 + \omega_S^2)^2 - 4(1-k^2)\omega_P^2\omega_S^2)^{1/2}$. The results are consistent with [18]. Considering ZVS condition of MOSFET $Q_{1,2,3,4}$, ω_H is usually used in the practical design. Then the CC for the diode rectifier at ω_H is given as

$$I_O|_{\theta=\pi,\omega=\omega_H} \approx \left|\frac{\omega_H M}{\omega_H^2 M^2 - \omega_H L_S\left(\omega_H L_P - \frac{1}{\omega_H C_P}\right)}\right| V_I \tag{12}$$

with R_P and R_S ignored.

To catch the high efficiency at R_{opt}, the CCSAR should have a gradually larger conduction angle θ until π with the supercapacitor charging time, that is the larger R_L, the larger θ. Then the normalized I_O curve varying with θ at ω_H is drawn as the blue solid curve in Fig. 7. Obviously, the output current of the SP IPT converter is not constant at the fixed frequency ω_H with the increasing R_L. To satisfy the required charging current, a variable frequency control is needed here. Fig. 7 also

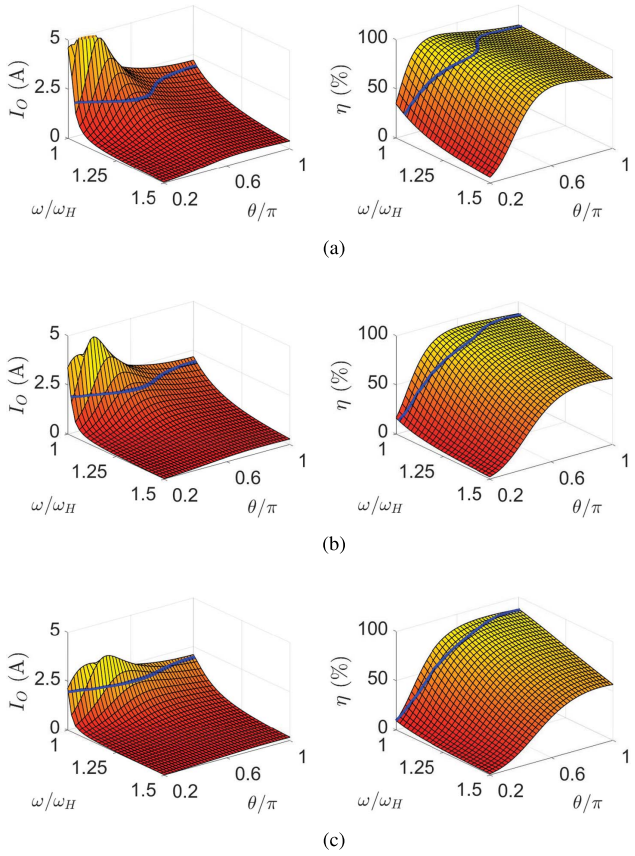

Fig. 8. Variations of output current $I_{\rm O}$ and power efficiency η with respect to operating frequency ω and conduction angle θ for different load conditions. (a) $R_{\rm L} = 15\ \Omega$. (b) $R_{\rm L} = 25\ \Omega$. (c) $R_{\rm L} = 45\ \Omega$.

gives the curves at the different operating frequencies larger than ω_H to ensure the ZVS of MOSFETs. As indicated by the arrows in red, the smaller the conduction angle θ, the higher the operating frequency ω, which can be tuned coordinately to maintain a CC output.

B. Bivariate Control

From (7) and (10), both output current $I_{\rm O}$ and transfer efficiency η are in relationship with ω, θ, and $R_{\rm L}$. For the purposes of CC charging and efficiency enhancement, a bivariate control with ω and θ coordinated operation under different load conditions should be given in theory. However, it is not available to get the analytical solution due to the high order equations. Then, the numerical calculation is used to derived all the operating points for different load conditions during the whole CC charging process. It can be carried out to find all the sets of (ω, θ) that achieve $I_{\rm O}|_{\theta=\pi,\omega=\omega_H}$ for each load condition, and then substitute all the sets of (ω, θ) into (7) to exhaustively search for the best efficiency points. Such that, the operating points can be found to achieve CC output and enhance the efficiency to the best.

Fig. 8 (left) demonstrates an example of operating points (ω, θ) for achieving the required 2-A current for the different loads. Parameters used in calculation are given as follows: $L_P = 62\ \mu$H, $L_S = 40\ \mu$H, $k = 0.29$, $R_P = 0.42\ \Omega$, $R_S = 0.27\ \Omega$, $C_{\rm P} = 83.8$ nF, and $C_{\rm S} = 118.8$ nF. Unless specified otherwise, they will be used for analysis in the rest of this

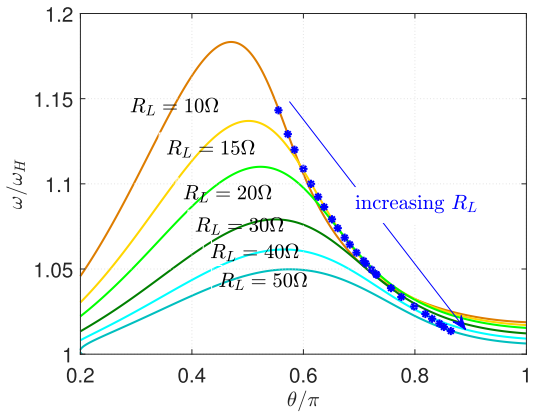

Fig. 9. Curves of ω and θ providing the required CC output at $I_{\rm O}|_{\theta=\pi,\omega=\omega_H} = 2$ A under different loads, where the blue dots are the optimum operating points with the optimum efficiency.

article. Fig. 8 (right) plots the efficiency traces under such pairs of (ω, θ) in Fig. 8 (left). In this way, the maximum efficiency can be found and marked in a 2-D space as shown in Fig. 9. Here, the solid curves in different colors represent possible solutions to achieve constant $I_{\rm O}|_{\theta=\pi,\omega=\omega_H}$ for different load conditions. Points marked with "$*$" are the optimum operating points enhancing the efficiency for R_L varying from 10 Ω to 50 Ω as indicated by the arrow direction.

With the operation illustrated above, the wide-range supercapacitor resistance $R_{\rm L}$ is transformed into equivalent resistance $R_{\rm eq}$ and the generation of $X_{\rm eq}$ changes the secondary resonant tank. To quantitatively evaluate their influence on efficiency enhancement, ($R_{\rm eq}/R_{\rm opt}$) and ($|X_{L_S} + X_{C_{\rm S,eq}}|/R_{\rm opt}$) in relationship with the variation of $R_{\rm L}$ are plotted in Fig. 10(a). It can be observed that, $R_{\rm eq}$ is about $0.5R_{\rm opt}$, while $|X_{L_S} + X_{C_{\rm S,eq}}|$ is less than $0.05R_{\rm opt}$. From Fig. 10(b), the SP IPT converter can achieve maximum efficiency when operating at secondary resonant frequency, i.e., $|X_{L_S} + X_{C_{\rm S,eq}}| = 0$ and loading at optimum resistance, i.e., $R_{\rm eq} = R_{\rm opt}$. The efficiency will decrease with the increase of $|X_{L_S} + X_{C_{\rm S,eq}}|$ and the deviation of $R_{\rm opt}$. As indicated by the red curve in Fig. 10(b), the efficiency of the conventional SP IPT converter without CCSAR degrades significantly due to the derivation of the load resistance. However, with the proposed bivariate coordinated control, the SP IPT converter with CCSAR can operate at approximately resonant frequency (i.e., ($|X_{L_S} + X_{C_{\rm S,eq}}|/R_{\rm opt}$) is close to 0) and load at nearly optimum resistance (i.e., ($R_{\rm eq}/R_{\rm opt}$) is not deviated too much) against the variation of $R_{\rm L}$. Such that, its efficiency can always locate in the blue region in Fig. 10(b), where efficiency enhancement can be achieved compared with the red curve.

Fig. 11 shows an efficiency comparison between the proposed SP IPT converter with CCSAR developed in this article and the conventional SP IPT converter with diode rectifier. Without considering converter losses, the SP IPT converter with CCSAR can achieve obvious efficiency enhancement throughout the whole load range.

C. Implementation

From Section II and Fig. 4, the conduction angle θ of $S_{6,8}$ should be controlled to improve the efficiency. Since the

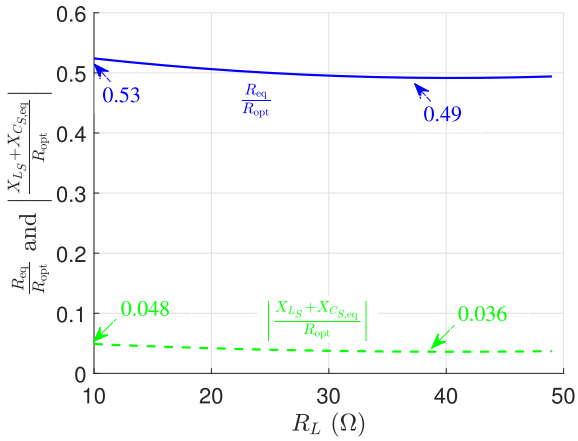

(a)

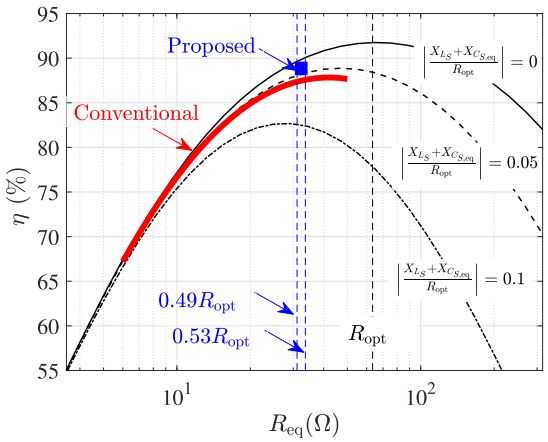

(b)

Fig. 10. (a) Quantitative evaluation of the equivalent load resistance R_{eq} and the reactance of the secondary resonant tank $|X_{L_S} + X_{C_{S,eq}}|$. (b) Analysis of efficiency enhancement.

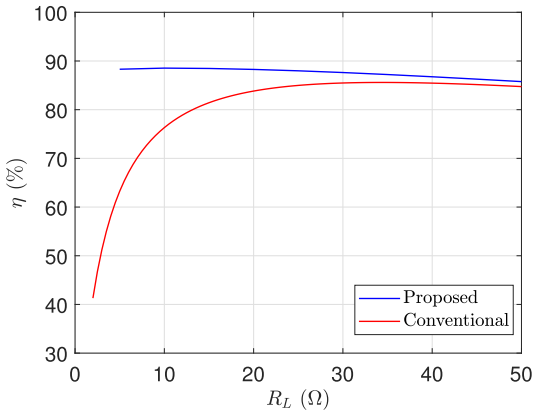

Fig. 11. Efficiency comparison between the proposed approach in this article and the conventional method in [18].

relationship between operating frequency ω and conduction angle θ is monotonic in Fig. 9, a simple current-loop PI controller is applied to correct the difference between I_O and $I_{O,ref}$, and the frequency modulation in the inverter is feasibly carried out with the optimum operating point sets of (ω, θ), which can be implemented by micro-controller with the

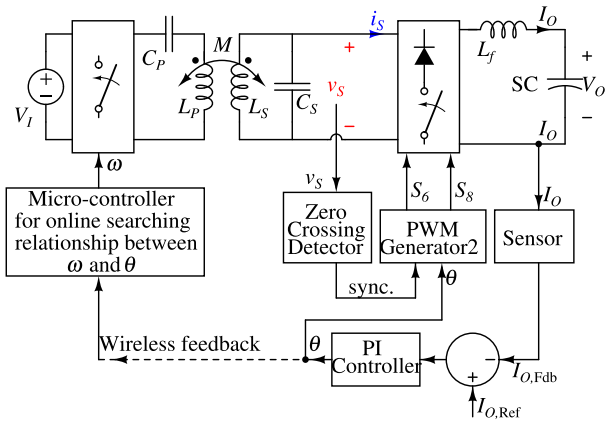

Fig. 12. Diagram of coordinated control.

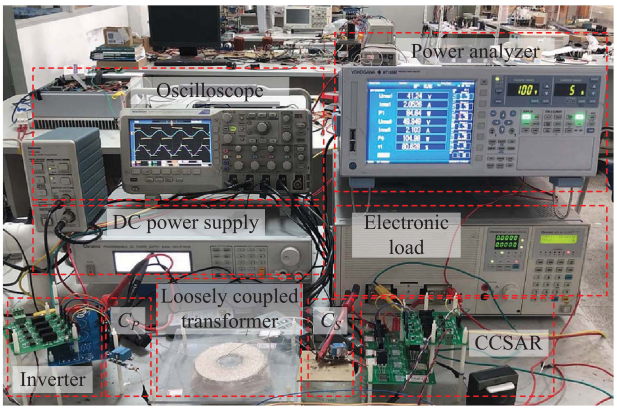

Fig. 13. Photograph of experimental prototype.

on-line derivation. In such a way, the required CC charging and efficiency enhancement can be synchronously realized.

Fig. 12 shows the coordinated control diagram in practical implementation. In the secondary side, besides the current-loop control, zero crossing detection of v_S generates a synchronization signal for the PWM generation. Thus, the proposed SP IPT converter can achieve a fast, direct, and precise control of the output current by modulating θ on the secondary side for CC charging, regardless of wireless communication. Meanwhile, in the primary side, the operating frequency varies with the variation of θ to achieve efficiency enhancement and it can be modulated in a slower manner due to the slow charging process of the supercapacitor. Commercially available 2.4G wireless communication can support frequency modulation. Instantaneous and slight frequency deviation on the primary side, which may be incurred by the delay of wireless communication, is allowed because it will only affect the real-time efficiency optimization and is not harmful to the output regulation. Thus, the frequency control on the primary side has low real-time dependence.

IV. Experimental Verification

To verify the CC output and efficiency performance of the proposed approach, an experimental prototype is built as shown in Fig. 13. The converter parameters and the charging specifications are given in Table I. The loosely-coupled transformer is constructed by two circular pads with the primary outer diameter of 60 mm and secondary outer diameter

TABLE I
SYSTEM PARAMETERS

System Parameters	Symbols	Values
Input voltage	V_I	50 V
Charging voltage	V_O	20–100 V
Charging current	I_O	2 A
	Q_1-Q_4,	IPP60R165
Switch	D_5, D_7	MBR20200
	S_6, S_8	IKP15N65F5 and MBR20200
Inductance	L_P, L_S	61.9 μH, 39.8 μH
Coupling coefficient	k	0.294
Coil resistance	R_P, R_S	0.5 Ω, 0.38 Ω
Capacitance	C_P, C_S	84.1 nF, 119.4 nF

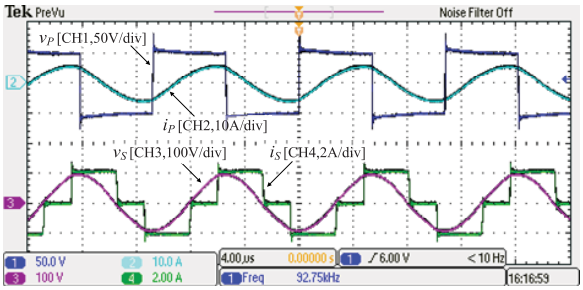

(a)

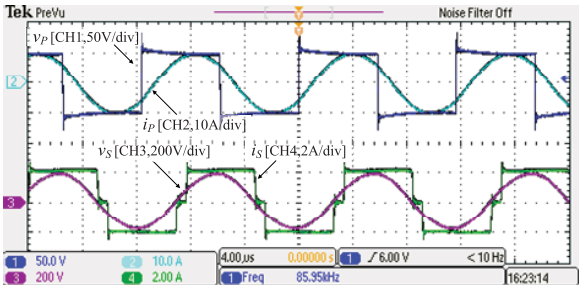

(b)

Fig. 14. Waveforms of the inverter and the active rectifier circuits at (a) $R_{\mathrm{L}} = 15\ \Omega$ and (b) $R_{\mathrm{L}} = 50\ \Omega$.

of 52 mm. The air gap is 30 mm. According to the charging current and the charging voltage, the equivalent supercapacitor resistance ranges from 10 to 50 Ω. An electronic load (Chroma 6314A) is used to emulate the supercapacitor. The dc-to-dc efficiency is measured by a power analyzer (YOKOGAWA WT1806E).

Following the proposed bivariate control in Section III-B, conduction angle θ of the CCSAR and operating frequency ω of the inverter are adjusted to achieve CC output with enhanced efficiency performance. Waveforms of the inverter and the active rectifier near the start ($R_{\mathrm{L}} = 15\ \Omega$) and at the end ($R_{\mathrm{L}} = 50\ \Omega$) of CC charging are shown in Fig. 14(a) and (b), respectively. As the operating waveforms are consistent with the analysis in Section II, ZCS is achievable in the CCSAR. The closed-loop control demonstrated in Section III-C has been implemented for CC charging. Transient waveforms for step changing of load resistance are shown in Fig. 15. The output voltage V_{O} and current I_{O} are measured and shown as CH2 in light blue and CH1 in dark blue. The control

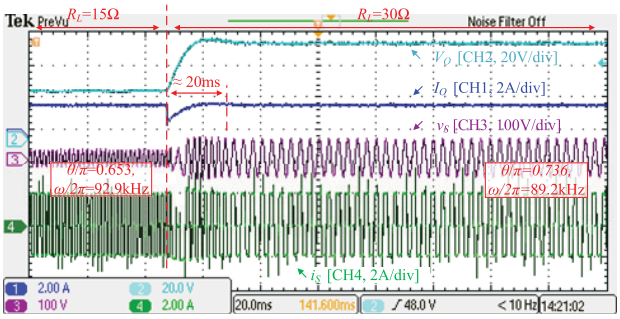

Fig. 15. Transient waveforms for R_{L} step changing from 15 to 30 Ω.

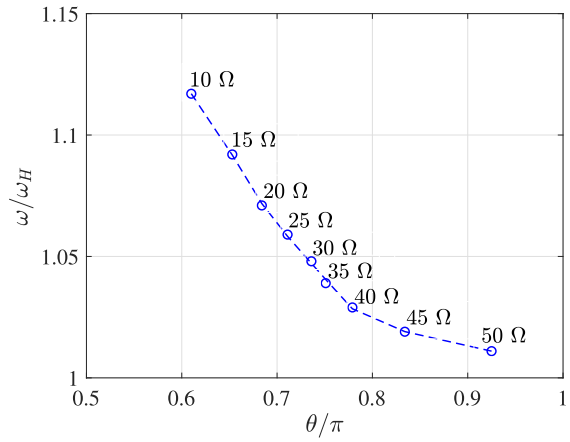

Fig. 16. Measured operating points at a fixed current output of 2 A and the corresponding load resistances.

variables are observed from CH3 in magenta and CH4 in green represent the conduction angle θ and the operating frequency ω, respectively. It can be observed that I_{O} is tightly regulated by the fast, direct and precise control of θ in the secondary within 20 ms. Slower control of ω in the transmitter side is based on the wireless feedback of the load information and can be observed according to the variation of the period of v_S and i_S.

The measured operating points (marked with "◯") are shown in Fig. 16, with ω and θ varying from 85 to 95 kHz and from 0.58π (104.4°) to 0.93π (167.4°), respectively. The corresponding output current (marked with "□") is kept at 2 A, as shown in Fig. 17(a). The output curent satisfies the requirement of CC charging. The measured efficiency points of the whole charging process are shown in Fig. 17(b). For a fair comparison, we have implemented both our proposed method and the method in [18] to achieve a CC output in an identical experiment prototype. The measured efficiency points using the proposed method (marked with "◯") are enhanced compared with the measured efficiency points (marked with "△") using the conventional scheme [18], which appears significant efficiency degradation at light load conditions. Compared to Fig. 11, the lower efficiency at light load conditions with the proposed approach is mainly attributed to the practical inverter and rectifier diode losses. To sum up, the efficiency can be enhanced during the CC charging process of the supercapacitor.

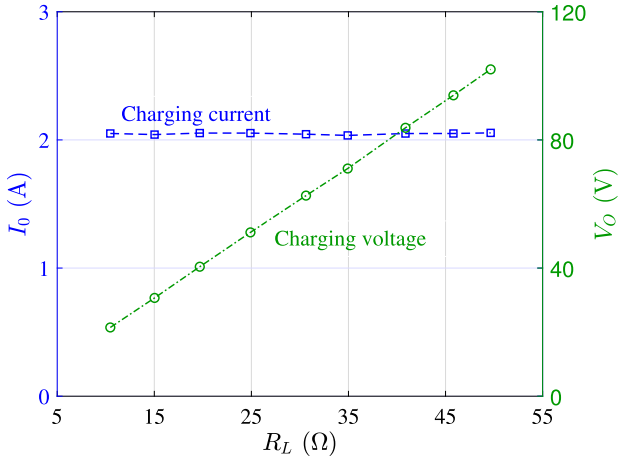

(a)

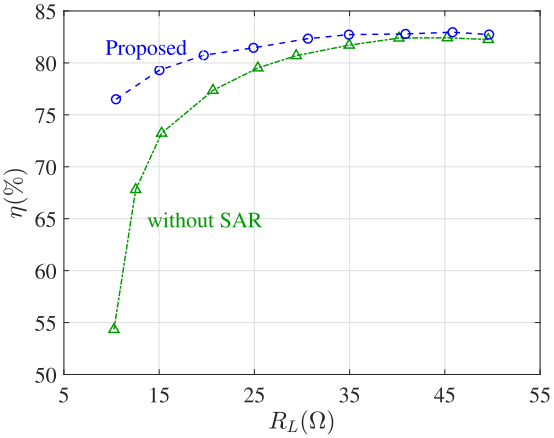

(b)

Fig. 17. (a) Measured output current and voltage versus supercapacitor resistance. (b) Comparison of measured efficiency between the proposed approach and the method (without SAR) in [18].

V. Conclusion

To improve the efficiency throughout a whole supercapacitor CC charging, this article proposes a novel CCSAR-based IPT converter. CCSAR is proven to comply with the required step-up load transformation by controlling the conduction angle of the CCSAR for efficiency enhancement. The desired charging CC can be regulated by tuning the operating frequency of the IPT inverter. A bivariate control is then adopted to coordinate these two objectives and achieve a precise current output with enhanced efficiency performance over the whole load range during the CC charging process. Finally, experiment results agree well with the theoretical analysis.

References

[1] S. Y. R. Hui, W. Zhong, and C. K. Lee, "A critical review of recent progress in mid-range wireless power transfer," *IEEE Trans. Power Electron.*, vol. 29, no. 9, pp. 4500–4511, Sep. 2014.

[2] S. Y. Hui, "Planar wireless charging technology for portable electronic products and Qi," *Proc. IEEE*, vol. 101, no. 6, pp. 1290–1301, Jun. 2013.

[3] Y. Yang, W. Zhong, S. Kiratipongvoot, S.-C. Tan, and S. Y. R. Hui, "Dynamic improvement of series–series compensated wireless power transfer systems using discrete sliding mode control," *IEEE Trans. Power Electron.*, vol. 33, no. 7, pp. 6351–6360, Jul. 2018.

[4] W. X. Zhong, X. Liu, and S. Y. R. Hui, "A novel single-layer winding array and receiver coil structure for contactless battery charging systems with free-positioning and localized charging features," *IEEE Trans. Ind. Electron.*, vol. 58, no. 9, pp. 4136–4144, Sep. 2011.

[5] D. Ahn and S. Hong, "Wireless power transmission with self-regulated output voltage for biomedical implant," *IEEE Trans. Ind. Electron.*, vol. 61, no. 5, pp. 2225–2235, May 2014.

[6] U. K. Madawala and D. J. Thrimawithana, "A bidirectional inductive power interface for electric vehicles in V2G systems," *IEEE Trans. Ind. Electron.*, vol. 58, no. 10, pp. 4789–4796, Oct. 2011.

[7] S. Lukic and Z. Pantic, "Cutting the cord: Static and dynamic inductive wireless charging of electric vehicles," *IEEE Electrific. Mag.*, vol. 1, no. 1, pp. 57–64, Sep. 2013.

[8] M. Zandi, A. Payman, J.-P. Martin, S. Pierfederici, B. Davat, and F. Meibody-Tabar, "Energy management of a fuel cell/supercapacitor/battery power source for electric vehicular applications," *IEEE Trans. Veh. Technol.*, vol. 60, no. 2, pp. 433–443, Feb. 2011.

[9] P. Kreczanik, P. Venet, A. Hijazi, and G. Clerc, "Study of supercapacitor aging and lifetime estimation according to voltage, temperature, and RMS current," *IEEE Trans. Ind. Electron.*, vol. 61, no. 9, pp. 4895–4902, Sep. 2014.

[10] A.-H. Hussein and I. Batarseh, "A review of charging algorithms for nickel and lithium battery chargers," *IEEE Trans. Veh. Technol.*, vol. 60, no. 3, pp. 830–838, Mar. 2011.

[11] D. Shin, Y. Kim, Y. Wang, N. Chang, and M. Pedram, "Constant-current regulator-based battery-supercapacitor hybrid architecture for high-rate pulsed load applications," *J. Power Sour.*, vol. 205, pp. 516–524, May 2012.

[12] Y. Parvini, A. Vahidi, and S. A. Fayazi, "Heuristic versus optimal charging of supercapacitors, lithium-ion, and lead-acid batteries: An efficiency point of view," *IEEE Trans. Control. Syst. Technol.*, vol. 26, no. 1, pp. 167–180, Jan. 2018.

[13] H. Li, J. Peng, J. He, Z. Huang, and J. Wang, "Observer-driven charging of supercapacitors," *IEEE Trans. Ind. Informat.*, vol. 16, no. 5, pp. 3439–3450, May 2020.

[14] Z. Li, K. Song, J. Jiang, and C. Zhu, "Constant current charging and maximum efficiency tracking control scheme for supercapacitor wireless charging," *IEEE Trans. Power Electron.*, vol. 33, no. 10, pp. 9088–9100, Oct. 2018.

[15] W. X. Zhong and S. Y. R. Hui, "Maximum energy efficiency tracking for wireless power transfer systems," *IEEE Trans. Power Electron.*, vol. 30, no. 7, pp. 4025–4034, Jul. 2015.

[16] Z. Huang, S.-C. Wong, and C. K. Tse, "Control design for optimizing efficiency in inductive power transfer systems," *IEEE Trans. Power Electron.*, vol. 33, no. 5, pp. 4523–4534, May 2018.

[17] W. Zhang, S.-C. Wong, C. K. Tse, and Q. Chen, "Analysis and comparison of secondary series- and parallel-compensated inductive power transfer systems operating for optimal efficiency and load-independent voltage-transfer ratio," *IEEE Trans. Power Electron.*, vol. 29, no. 6, pp. 2979–2990, Jun. 2014.

[18] W. Zhang, S.-C. Wong, C. K. Tse, and Q. Chen, "Load-independent duality of current and voltage outputs of a series- or parallel-compensated inductive power transfer converter with optimized efficiency," *IEEE J. Emerg. Sel. Topics Power Electron.*, vol. 3, no. 1, pp. 137–146, Mar. 2015.

[19] X. Qu, W. Zhang, S.-C. Wong, and C. K. Tse, "Design of a current-source-output inductive power transfer LED lighting system," *IEEE J. Emerg. Sel. Topics Power Electron.*, vol. 3, no. 1, pp. 306–314, Mar. 2015.

[20] Y. Wang, Y. Yao, X. Liu, D. Xu, and L. Cai, "An LC/S compensation topology and coil design technique for wireless power transfer," *IEEE Trans. Power Electron.*, vol. 33, no. 3, pp. 2007–2025, Mar. 2018.

[21] Z. Huang, S. C. Wong, and C. K. Tse, "Design of a single-stage inductive-power-transfer converter for efficient EV battery charging," *IEEE Trans. Veh. Technol.*, vol. 66, no. 7, pp. 5808–5821, Jul. 2017.

[22] V.-B. Vu, D.-H. Tran, and W. Choi, "Implementation of the constant current and constant voltage charge of inductive power transfer systems with the double-sided LCC compensation topology for electric vehicle battery charge applications," *IEEE Trans. Power Electron.*, vol. 33, no. 9, pp. 7398–7410, Sep. 2018.

[23] X. Qu, Y. Yao, D. Wang, S.-C. Wong, and C. K. Tse, "A family of hybrid IPT topologies with near load-independent output and high tolerance to pad misalignment," *IEEE Trans. Power Electron.*, vol. 35, no. 7, pp. 6867–6877, Jul. 2020.

[24] Z. Huang, S.-C. Wong, and C. K. Tse, "Comparison of basic inductive power transfer systems with linear control achieving optimized efficiency," *IEEE Trans. Power Electron.*, vol. 35, no. 3, pp. 3276–3286, Mar. 2020.

[25] M. Fu, H. Yin, X. Zhu, and C. Ma, "Analysis and tracking of optimal load in wireless power transfer systems," *IEEE Trans. Power Electron.*, vol. 30, no. 7, pp. 3952–3963, Jul. 2015.

[26] T.-D. Yeo, D. Kwon, S.-T. Khang, and J.-W. Yu, "Design of maximum efficiency tracking control scheme for closed-loop wireless power charging system employing series resonant tank," *IEEE Trans. Power Electron.*, vol. 32, no. 1, pp. 471–478, Jan. 2017.

[27] Y. Yang, S. C. Tan, and S. Y. R. Hui, "Fast hardware approach to determining mutual coupling of series–series-compensated wireless power transfer systems with active rectifiers," *IEEE Trans. Power Electron.*, vol. 35, no. 10, pp. 11026–11038, Oct. 2020.

[28] T. Diekhans and R. W. D. Doncker, "A dual-side controlled inductive power transfer system optimized for large coupling factor variations and partial load," *IEEE Trans. Power Electron.*, vol. 30, no. 11, pp. 6320–6328, Nov. 2015.

[29] Q. Chen, L. Jiang, J. Hou, X. Ren, and X. Ruan, "Research on bidirectional contactless resonant converter for energy charging between EVs," in *Proc. 39th Annu. Conf. IEEE Ind. Electron. Soc.*, Vienna, Austria, Nov. 2013, pp. 1236–1241.

[30] K. Colak, E. Asa, M. Bojarski, D. Czarkowski, and O. C. Onar, "A novel phase-shift control of semibridgeless active rectifier for wireless power transfer," *IEEE Trans. Power Electron.*, vol. 30, no. 11, pp. 6288–6297, Nov. 2015.

[31] T. Mishima and E. Morita, "High-frequency bridgeless rectifier based ZVS multiresonant converter for inductive power transfer featuring high-voltage GaN-HFET," *IEEE Trans. Ind. Electron.*, vol. 64, no. 11, pp. 9155–9164, Nov. 2017.

[32] Z. Huang, S.-C. Wong, and C. K. Tse, "An inductive-power-transfer converter with high efficiency throughout battery-charging process," *IEEE Trans. Power Electron.*, vol. 34, no. 10, pp. 10245–10255, Oct. 2019.

[33] G. Ivensky, I. Zeltser, A. Kats, and S. Ben-Yaakov, "Reducing IGBT losses in ZCS series resonant converters," *IEEE Trans. Ind. Electron.*, vol. 46, no. 1, pp. 67–74, Feb. 1999.

[34] M. Takei, Y. Harada, and K. Ueno, "600 V-IGBT with reverse blocking capability," in *Proc. Int. Sym. Power Semicond. Dev. IC's*, 2001, pp. 413–416.

[35] N. Iwamuro and T. Laska, "IGBT history, state-of-the-art, and future prospects," *IEEE Trans. Electron Dev.*, vol. 64, no. 3, pp. 741–752, Mar. 2017.

Zhicong Huang (Member, IEEE) received the B.Eng. degree in electrical engineering and automation and the M.Eng. degree in mechanical and electronic engineering from Huazhong University of Science and Technology, Wuhan, China, in 2010 and 2013, respectively, and the Ph.D. degree in power electronics from The Hong Kong Polytechnic University, Hong Kong, in 2018.

He is currently an Assistant Professor with Shien-Ming Wu School of Intelligent Engineering, South China University of Technology, Guangzhou, China. His research interests include wireless power transfer, electric vehicle, and intelligent engineering.

Dr. Huang was a recipient of the UM Macao Talent Program in 2018. He received the Best Track Paper from IEEE Asia-Pacific Power and Energy Engineering Conference (APPEEC) in 2019.

Dule Wang received the B.Eng. degree from Jiangsu University, Zhenjiang, China, in 2017, and the M.Eng. degree from Southeast University, Nanjing, China, in 2020, all in electrical engineering.

He is currently working with State Grid Corporation of China, Lianyungang, China. His current research interest includes wireless power transfer.

Xiaohui Qu (Senior Member, IEEE) received the B.Eng. and M.Eng. degrees in electrical engineering from Nanjing University of Aeronautics and Astronautics, Nanjing, China, in 2003 and 2006, respectively, and the Ph.D. degree in power electronics from The Hong Kong Polytechnic University, Hong Kong, in 2010.

From February 2009 to May 2009, she was engaged as a Visiting Scholar with the Center for Power Electronics Systems, Virginia Tech, Blacksburg, VA, USA. In 2010, she joined the School of Electrical Engineering, Southeast University, Nanjing, where she is currently a Full Professor with a research focus on power electronics. From January 2015 to January 2016, she was a Visiting Scholar with the Center of Reliable Power Electronics (CORPE), Aalborg University, Aalborg, Denmark. Her current research interests include LED lighting systems, wireless power transfer, and power electronics reliability.

Dr. Qu received the Outstanding Reviewer Award and the Prize Paper Award from IEEE TRANSACTIONS ON POWER ELECTRONICS in 2017 and 2018, respectively. She has been an Associate Editor of the IEEE TRANSACTIONS ON POWER ELECTRONICS since 2020.